

# Low-Energy $\Lambda - p$ Scattering Parameters from the $pp \rightarrow pK^+\Lambda$ Reaction

J.T. Balewski<sup>1,2</sup>, A. Budzanowski<sup>1</sup>, C. Goodman<sup>3</sup>, D. Grzonka<sup>2</sup>, M. Hofmann<sup>2</sup>,  
L. Jarczyk<sup>4</sup>, A. Khoukaz<sup>5</sup>, K. Kilian<sup>2</sup>, T. Lister<sup>5</sup>, P. Moskal<sup>2,4</sup>, W. Oelert<sup>2</sup>, I.A. Pellmann<sup>2,5</sup>,  
C. Quentmeier<sup>5</sup>, R. Santo<sup>5</sup>, G. Schepers<sup>5</sup>, T. Sefzick<sup>2</sup>, S. Sewerin<sup>2</sup>, J. Smyrski<sup>4</sup>,  
A. Strzałkowski<sup>4</sup>, C. Thomas<sup>5</sup>, C. Wilkin<sup>6</sup>, M. Wolke<sup>2</sup>, P. Wüstner<sup>7</sup>, D. Wyrwa<sup>2,4</sup>

<sup>1</sup> *Institute of Nuclear Physics, Cracow, Poland*

<sup>2</sup> *IKP, Forschungszentrum Jülich, Germany*

<sup>3</sup> *IUCF, Bloomington, Indiana, USA*

<sup>4</sup> *Institute of Physics, Jagellonian University, Cracow, Poland*

<sup>5</sup> *IKP, Westfälische Wilhelms-Universität, Münster, Germany*

<sup>6</sup> *University College London, London WC1E 6BT, United Kingdom*

<sup>7</sup> *ZEL, Forschungszentrum Jülich, Germany*

## Abstract

Constraints on the spin-averaged  $\Lambda p$  scattering length and effective range have been obtained from measurements of the  $pp \rightarrow pK^+\Lambda$  reaction close to the production threshold by comparing model phase-space Dalitz plot occupations with experimental ones. The data fix well the position of the virtual bound state in the  $\Lambda p$  system. Combining this with information from elastic  $\Lambda p$  scattering measurements at slightly higher energies, together with the fact that the hyperdeuteron is not bound, leads to a new determination of the low energy  $\Lambda p$  scattering parameters.

**PACS:** 12.38.Qk, 13.85.Hd, 25.40.Ve

**Keywords:** scattering length, effective range, Dalitz plot

# 1 Introduction

The existence of light hypernuclei, such as  ${}^3_{\Lambda}\text{He}$ , shows the low energy  $\Lambda$ - $p$  interaction to be strongly attractive, though not sufficient to bind the two-baryon hyperdeuteron. The  $\Lambda$ - $p$  interaction is of especial interest since it is influenced by the strange quark content of the  $\Lambda$ -hyperon. However, in contrast to the nucleon-nucleon case, due to the short lifetime of the  $\Lambda$ , direct measurements of low-energy  $\Lambda$ - $p$  scattering are sparse and the resulting parameters rather poorly known.

Bubble chamber measurements [1, 2, 3], based on samples of a few hundred secondary events, have allowed determinations of the elastic cross section down to  $\Lambda$  laboratory momenta  $\approx 130$  MeV/ $c$ . In the low energy region, where only  $S$ -waves are important, the spin-averaged total cross section is of the form

$$\sigma_{\Lambda p \rightarrow \Lambda p} = \frac{\pi}{q^2 + \left(-1/a_s + \frac{1}{2}r_s q^2\right)^2} + \frac{3\pi}{q^2 + \left(-1/a_t + \frac{1}{2}r_t q^2\right)^2}. \quad (1)$$

Here  $q$  is the  $\Lambda p$  centre-of-mass momentum and  $a_{s(t)}$  and  $r_{s(t)}$  are, respectively, the  $S$ -wave scattering lengths and effective ranges in the  $\Lambda p$  spin-singlet and triplet states. Separate values of these parameters have been claimed for the two spin states [1, 2] and these are shown in Fig. 1. However, the error bars are large, strongly and systematically correlated and hard to quantify, since such data should really only support the determination of an average scattering length  $\bar{a}$  and effective range  $\bar{r}$  [3]. Already for laboratory momenta  $\approx 300$  MeV/ $c$ , the differential cross section is significantly non-isotropic, indicating the presence of  $P$  or higher waves [1, 2], and so it is not surprising that the  $S$ -wave parameters deduced from such experiments depend upon the upper momentum cut assumed.

Values of the scattering length and effective range have also been deduced through the study of the  $\Lambda p$  final state interaction (FSI) in the  $K^- d \rightarrow \pi^- p \Lambda$  reaction with stopped  $K$ -mesons [4]. Here it is the shape of the  $\Lambda p$  effective mass spectrum near the kinematic limit which is sensitive to the parameters. In impulse approximation the amplitude for this process is proportional to that for  $K^- n \rightarrow \pi^- \Lambda$  and, if the Fermi motion in the target deuteron is neglected, the reaction is purely  $s$ -wave with no spin-flip. The final  $\Lambda p$  system is therefore in the same spin-triplet state as the  $np$

pair in the deuteron and the values  $a_t$  and  $r_t$  so determined, which are also shown in Fig. 1, are consistent with those obtained from the scattering experiments [1, 2].

Phenomenological investigations of the  $\Lambda p$  interaction by the Jülich [5] and Nijmegen [6] groups yield low energy scattering parameters in agreement with the results of Fig. 1, though it is impossible to quantify the systematic uncertainties inherent in such models. It should, however, be noted that their spin-singlet potential is more attractive than the triplet, which is necessary to ensure the correct spin assignments of the ground states of  ${}^3_{\Lambda}\text{H}$  and  ${}^4_{\Lambda}\text{He}$  [7].

The final state interaction in the  $pp \rightarrow K^+ p \Lambda$  reaction at low  $\Lambda p$  effective masses is also sensitive to the  $\Lambda p$  scattering parameters [8]. The recent data on this reaction very close to threshold [9], taken at the COSY-11 magnetic spectrometer [10] installed at the cooler synchrotron COSY-Jülich [11], allow us to extract information complementary to that obtained from elastic scattering because it is possible to reach lower centre-of-mass momenta.

In the present paper we aim to constrain the  $\Lambda p$  scattering parameters from the shapes of the double-differential  $pp \rightarrow K^+ p \Lambda$  cross section. In section 2 a simplified model is outlined to describe the principal interactions between the three outgoing particles. Experimental details, including event selection, are discussed in section 3. The FSI model was already used in ref. [9] to determine the precise beam energy by fitting the integrated total cross sections as a function of beam energy with assumed values of the  $\Lambda p$  input parameters. To avoid biasing the analysis, in the present work we determine the  $\Lambda p$  parameters using only the structure of the Dalitz plot at each energy and not its normalisation. For this purpose we apply the maximum likelihood method to obtain a map of the confidence levels for the  $\Lambda p$  scattering parameters. This formalism and the definition of the event weights are shown in section 4. Even taking the  $\Lambda p$  spin-triplet and singlet to be identical, the resulting values of the average scattering length and effective range presented in section 5 are strongly and systematically correlated in the fit, such that it is hard to quote error bars. However, the position of the nearby pole in the  $\Lambda p$  scattering amplitude, corresponding to a virtual bound state of the system, is much more stable, being unbound by  $(7.7^{+6.0}_{-3.0})$  MeV. Our conclusions are presented in section 6.

## 2 Model for the FSI in the $pp \rightarrow pK^+\Lambda$ reaction

As discussed in ref. [9], if the basic production mechanism is of short range then the energy dependence of the  $pp \rightarrow pK^+\Lambda$  cross section close to threshold is dominated by the available three-body phase-space  $d\rho(3)$ , modified by final-state interactions. In principle one should consider FSI's in all the three two-body subsystems,  $\Lambda$ - $p$ ,  $\Lambda$ - $K$ , and  $p$ - $K$ . Since the strong interaction in the first case appears to be more than an order of magnitude larger than for the other two [12, 13], we concentrate on the dominant factor  $f_{FSI}(q)$  in the  $\Lambda$ - $p$  system. In addition, however, the Coulomb repulsion in the proton-kaon subsystem  $f_c(q_{pK})$ , where  $q_{pK}$  denotes the c.m. momentum in  $pK$  subsystem, is also important at the low energies pertaining in our experiment. Keeping only these two interactions our *ansatz* for the production cross section is

$$d\sigma \sim f_c(q_{pK}) f_{FSI}(q) d\rho(3). \quad (2)$$

The  $S$ -wave assumption implicit here is justified for our experiment since, for excess energies  $\varepsilon < 7$  MeV, the maximum momentum in any two-body subsystem is below 100 MeV/c. It should be noted that the bubble chamber data [1, 2] cover a higher range of  $\Lambda$ - $p$  momenta.

Choosing as independent variables  $S_{pK}$  and  $S_{\Lambda K}$ , the squares of the effective masses in the  $p$ - $K$  and  $\Lambda$ - $K$  subsystems, integration of Eq. (2) over the angular variables leads to a number of events per pixel in the Dalitz plot distribution of the form

$$\frac{d^2\sigma}{dS_{pK} dS_{\Lambda K}} \sim \int_{\text{angles}} f_c(q_{pK}) f_{FSI}(q) d\rho(3). \quad (3)$$

Structure in the Dalitz plot must be associated with the functions  $f_{FSI}$  and  $f_c$ . Now the Coulomb distortion factor defined in Ref. [9] contains no free parameters [14]. In contrast the  $f_{FSI}$  factor depends on the scattering lengths and effective ranges in the triplet and singlet states. Since the spin dependence is expected to be small [5, 6], as shown by some of the extracted numbers in Fig. 1, and our experiment is not sensitive to singlet/triplet differences, we used mean values of the

scattering length  $\bar{a}$  and effective range  $\bar{r}$  in the parametrization of  $f_{FSI}$ . In analogy with Eq. (1), we take the popular Watson form for the final state interaction [15]

$$f_{FSI}(q, \bar{a}, \bar{r}) = \frac{1}{\bar{a}^2 q^2 + \left(-1 + \frac{1}{2}\bar{r}\bar{a}q^2\right)^2}. \quad (4)$$

A typical Dalitz plot distribution calculated from Eqs. (3) and (4) with  $\bar{a} = -1.6$  fm and  $\bar{r} = 2.3$  fm is shown in Fig. 2.

### 3 Experiment

The measurement of the  $pp \rightarrow pK^+\Lambda$  reaction was performed at the COSY-Jülich synchrotron, using the internal target facility COSY-11 [10]. Outgoing protons and positively charged kaons were identified by means of particle momentum reconstruction in the magnetic field combined with time-of-flight measurement. The four-momentum, and hence the missing mass (MM), corresponding to the unobserved  $\Lambda$ -hyperon was calculated from energy-momentum conservation. Details of the experimental technique are given elsewhere [16].

An example of the missing mass spectrum is shown in Fig. 3. The function  $G(MM)$  used to fit the peak corresponding to good  $pp \rightarrow pK^+\Lambda$  events, is combined with the smooth background  $B(MM)$ . Only events which deviate by less than  $\pm 2\sigma$  from the central value were accepted and a weight  $w = G(MM)/[G(MM) + B(MM)]$  was assigned to each of them to describe the probability that the particular event resulted from a  $pK^+\Lambda$  final state rather than being a background signal. Our data were well described by a Gaussian form for  $G(MM)$  with  $\sigma = 0.5$  MeV. The closer  $MM$  is to the known  $\Lambda$  mass  $m_\Lambda$ , the larger the weight  $w$  for the event. Thus  $w$  can be interpreted as a penalty factor which is imposed on events where the observables are significantly modified by the application of the kinematic fit procedure.

The experimental Dalitz plot for  $\varepsilon = 4.7$  MeV, shown in Fig. 4a, demonstrates that the whole kinematically allowed region is occupied by data, so that there are no forbidden zones in our acceptance. This experimental acceptance, calculated *via* a Monte-Carlo simulation with a pure phase-space generator, is however non-uniform with a *Colosseum*-like pattern, as illustrated in Fig. 4b. Comparison of the

experimental Dalitz plot (Fig. 4a) with the model calculation (Fig. 2), folded with the detector acceptance (Fig. 4b), allows a determination of the model parameters  $\bar{a}$  and  $\bar{r}$  at each excess energy  $\varepsilon$ . Although they influence the statistical confidence, the relative counting rates at different  $\varepsilon$  are not used, which is important since the variation of cross section with energy has already been employed in fixing the absolute beam energy [9].

## 4 Fitting procedure

The maximum likelihood method was applied to determine best values of the  $\bar{a}$  and  $\bar{r}$  parameters, though it must be stressed that these will be strongly correlated due to the form of the  $f_{FSI}$  factor of Eq. (4). A set of model Dalitz plots  $D_{\bar{a},\bar{r}}(S_{pK}, S_{\Lambda K})$ , as defined in Eq. (3) and (4), was generated at fixed excess energy  $\varepsilon$  over a grid in  $(\bar{a}, \bar{r})$  with  $\bar{a} \in [-6, 6]$  fm and  $\bar{r} \in [0, 10]$  fm and a step-size of 0.2 fm in each variable.

Defining for brevity  $x \equiv S_{pK}$  and  $y \equiv S_{\Lambda K}$ , the probability  $\mathcal{P}$  that an event will be detected with some  $(x, y)$  value is

$$\mathcal{P}(x, y) = D_{\bar{a}, \bar{r}}(x, y) A(x, y) \bigg/ \int_{\text{Dalitz plot}} D_{\bar{a}, \bar{r}}(x, y) A(x, y) dx dy, \quad (5)$$

where  $A(x, y)$  is the acceptance function.

Applying the experimental event weight  $w_i$ , the likelihood of a single event is

$$l_i = [\mathcal{P}(x_i, y_i)]^{w_i} \equiv \mathcal{P}_i^{w_i}$$

and the corresponding global likelihood function

$$\mathcal{L}(\bar{a}, \bar{r}) = \prod_{i=1}^N \mathcal{P}_i^{w_i}. \quad (6)$$

Since  $w_i$  is the probability that the  $i$ -th event is a  $pK^+\Lambda$  and not a background reaction, if the whole experiment were repeated  $M$  times with perfect background subtraction, then each  $i$ -th event would appear  $M w_i$  times. The likelihood corresponding to each  $(x_i, y_i)$  point is given by  $l_i^* = \mathcal{P}_i^{M w_i}$  and the global likelihood function is:  $\mathcal{L}^* = \prod_{i=1}^N (\mathcal{P}_i)^{M w_i} = (\mathcal{L})^M$ .

Both likelihood functions  $\mathcal{L}(\bar{a}, \bar{r})$  and  $\mathcal{L}^*(\bar{a}, \bar{r})$  have their extrema at the same  $(\bar{a}_0, \bar{r}_0)$  points and thus it is sufficient to perform the experiment once, searching for the maximum of the  $\mathcal{L}(\bar{a}, \bar{r})$  function.

In order to amalgamate the likelihood functions from measurements at different values of  $\varepsilon$ , the  $M$  was chosen in such a way that  $M \sum w_i$  was equal to the number of measured events  $N$ .

As shown by Eadie [17], the quantity  $-2 \ln [\mathcal{L}(\bar{a}, \bar{r})/\mathcal{L}(\bar{a}_0, \bar{r}_0)]$  has an asymptotic  $\chi^2$  distribution corresponding to the two degrees of freedom, *i.e.* two parameters  $(\bar{a}, \bar{r})$ . The equation

$$\ln \mathcal{L}(\bar{a}, \bar{r}) = \ln \mathcal{L}(\bar{a}_0, \bar{r}_0) - \frac{1}{2} \chi^2_\beta(2) \quad (7)$$

defines two-dimensional contours in the  $(\bar{a}, \bar{r})$  plane for the desired confidence level  $\text{CL} = 1 - \beta$ .

## 5 Results

Contours in the  $(\bar{a}, \bar{r})$  plane of the global likelihood function calculated from a sample of about 2400 events measured at six excess energies from 2.7 to 6.7 MeV are shown in Fig. 5. Those solutions with a positive value of  $\bar{a}$  are to be excluded since they would imply the existence of a bound  $\Lambda p$  system and the hyperdeuteron has never been found. The branch with negative  $\bar{a}$  yields a long narrow ridge with a very strong correlation between the scattering length and effective range, such that it is only a combination of the two parameters which is well determined by the experiment. The averaged values from the literature [1]–[6] lie close to the ridge but generally slightly outside the 99%-confidence contour.

The parameter which is in fact well determined by this experiment is the energy of the nearby pole in the  $\Lambda p$  scattering amplitude. To see this, rewrite the final-state-interaction factor of Eq. (4) in the form

$$f_{FSI}(q; \bar{a}, \bar{r}) = \frac{\gamma_1^2 \gamma_2^2}{(q^2 + \gamma_1^2)(q^2 + \gamma_2^2)} . \quad (8)$$

The  $\Lambda p$  scattering amplitude has poles at  $q = i\gamma_n$ , where

$$\gamma_1 = \frac{1}{\bar{r}} \left[ 1 - \sqrt{1 - \frac{2\bar{r}}{\bar{a}}} \right] \quad \text{and} \quad \gamma_2 = \frac{1}{\bar{r}} \left[ 1 + \sqrt{1 - \frac{2\bar{r}}{\bar{a}}} \right]. \quad (9)$$

It is straightforward from Eq. (9) to transform the likelihood function into the new variables and the contours in the resulting  $\mathcal{L}(\gamma_1, \gamma_2)$  are shown in Fig. 6 together with the literature values [1]–[6]. Note that the functional form of Eq. (8) clearly shows that the data are sensitive only to the magnitudes of the  $\gamma_i$  and that the results must be symmetric under the interchange  $\gamma_1 \leftrightarrow \gamma_2$ . We therefore establish the convention that  $|\gamma_2| > |\gamma_1|$ . If  $\gamma_1$  is positive then that would correspond to a bound state of the  $\Lambda p$  system, whereas if it is negative then it is an antibound or virtual state of the kind with which one is familiar from the low energy proton-proton singlet  $S$ -wave. The two branches seen in the maximum likelihood contours of Fig. 5 correspond to the mere reversal of the sign of  $\gamma_1$ . Since it is highly unlikely that there would be another singularity of the  $\Lambda$ - $p$  amplitude very close to zero energy, we can assume that  $|\gamma_2| \gg |\gamma_1|$ , in which case we deduce from our fit that  $\gamma_1 = (-0.45_{-0.1}^{+0.15}) \text{ fm}^{-1}$ . It has been argued [18] that the single pole limit of letting  $\gamma_2 \rightarrow \infty$  in fact provides a better representation of  $f_{FSI}$  than the scattering length – effective range form of Eq. (4). Our value of  $\gamma_1$  corresponds to the average  $\Lambda$ - $p$  system being unbound by an amount  $(7.7_{-3.0}^{+6.0}) \text{ MeV}$ .

In order to obtain values of  $\bar{a}$  and  $\bar{r}$  separately, we must use extra experimental information such as for example  $\Lambda$ - $p$  elastic scattering cross section data. It is seen from Eq. (1) that the normalisation of this at zero energy is proportional to the square of the scattering length. The low energy data of Ref. [1, 2] are shown in Fig. 7 together with a fit to the data on the basis of Eq. (1), where the parameters  $\bar{a}$  and  $\bar{r}$  are constrained to lie on the maximum likelihood ridge of Fig. 6. This is achieved with  $\bar{a} = -2.0 \text{ fm}$  and  $\bar{r} = 1.0 \text{ fm}$ , corresponding to  $\gamma_1 = -0.41 \text{ fm}^{-1}$  and  $\gamma_2 = 2.4 \text{ fm}^{-1}$ . The fit therefore confirms that  $\gamma_2 \gg \gamma_1$  and that the  $\Lambda p$  scattering data do not realistically allow for a separation between singlet and triplet parameters. It is worth noting that our production data are sensitive to much lower values of  $\varepsilon$ , as indicated by the arrow, than the scattering data, and it is this region which



determines best the value of  $\gamma_1$  and hence the position of the pole of the virtual bound state.

## 6 Conclusions

Through an analysis of the two-dimensional structure of the Dalitz plot for the  $pp \rightarrow pK^+\Lambda$  reaction at fixed energies within a simple final-state-interaction model, we have established a strong constraint between the spin-averaged  $\Lambda p$  scattering length and effective range. The data allow us to fit accurately the position of the spin-average virtual bound state  $\gamma_1$ . Since the data were taken at excess energies which are inaccessible to low energy elastic scattering experiments, the results are complementary and it is appropriate to make a combined fit of the whole data set, leading to new values of  $(\bar{a}, \bar{r})$ .

The total cross section data of Ref. [9] have recently been analysed to determine values of  $(\bar{a}, \bar{r})$  [19]. Their argument is, however, somewhat cyclic since a final-state interaction with fixed scattering length and effective range was already used in the experimental analysis to fix the beam energy [9]. In principle therefore these values should then be found by the fitting procedure, though there are still of course the ambiguities discussed in this paper. We avoid falling into this trap by not using the relative normalisation of the event rate as a function of the beam energy within our fitting procedure. It is rather the structure of the two-dimensional Dalitz plots which fixes our parameter values.

Though we have implicitly assumed that the  $\Lambda p$  system produced from the near-threshold  $pp \rightarrow pK^+\Lambda$  reaction is the same 3:1 spin-average seen in bubble chamber scattering experiments, this is not guaranteed. Just as in the  $K^-$ -capture experiment [4], the basic reaction mechanism could favour the production of a particular spin combination in the final state. If the present experiment were extended through the use of a polarised beam and target, then it would be possible to repeat the current analysis separately in the singlet and triplet final states to separate these important quantities.

## Acknowledgements

We should like to thank Dr A. Szczurek for very helpful discussions. The research project was supported by the BMBF, the Polish Committee for Scientific Research, the Bilateral Cooperation between Germany and Poland, represented by the Internationales Büro DLR for the BMBF, and the FFE program of the Forschungszentrum Jülich. One of the authors (CW) is grateful to the FZ-Jülich for the consultancy which supported some of this work.

## References

- [1] G. Alexander et al., Phys. Rev. **173**, 1452 (1968)
- [2] B. Sechi-Zorn et al., Phys. Rev. **175**, 1735 (1968)
- [3] G. Alexander, Proc.Int.Conf. on Hypernuclei,  
Argonne National Laboratory, July 1969
- [4] Tai Ho Tan, Phys. Rev. Lett. **23**, 395 (1969)
- [5] B. Holzenkamp et al., Nucl. Phys. **A500**, 485 (1989);  
A. Reuber et al., Nucl. Phys. **A570**, 543 (1994)
- [6] M.M. Nagels et al., Phys. Rev. **D20**, 1633 (1979)
- [7] R.H. Dalitz, Nuclear Interactions of the Hyperons, Oxford,  
Oxford University Press, 1965
- [8] R. Siebert et al., Nucl.Phys. **A567**, 819 (1994);  
J.M. Laget, Phys.Lett. **B259**, 24 (1991)
- [9] J.Balewski et al., Phys. Lett. **B** (in press)
- [10] S. Brauksiepe et al., Nucl.Instr. and Meth. **A376**, 397 (1996)

- [11] U. Bechstedt et al., Nucl.Instr. and Meth. **B113**, 26 (1996);  
R. Maier, Nucl.Instr. and Meth. **A390**, 1 (1997)
- [12] M. Hoffmann et al., Nucl.Phys. **A593**, 341 (1995)
- [13] A. Deloff, Nucl.Phys. **A505** (1989) 583
- [14] C. Hanhart et al., Phys.Lett. **B358**, 21 (1995)
- [15] M.L. Goldberger and K.M. Watson, Collision Theory, New York,  
John Wiley & Sons, 1964
- [16] J.Balewski et al., Phys.Lett. **B388**, 859 (1996)
- [17] W.T.Eadie et al., Statistical Methods in Experimental Physics, Amsterdam,  
North-Holland Publishing Company, 1971
- [18] G. Fäldt and C. Wilkin, Phys.Lett. **B382**, 209 (1996);  
Z.Phys. **A357**, 241 (1997)
- [19] A. Sibirtsev and W. Cassing, University of Giessen preprint UGI-98-7  
(nucl-th/9802025)

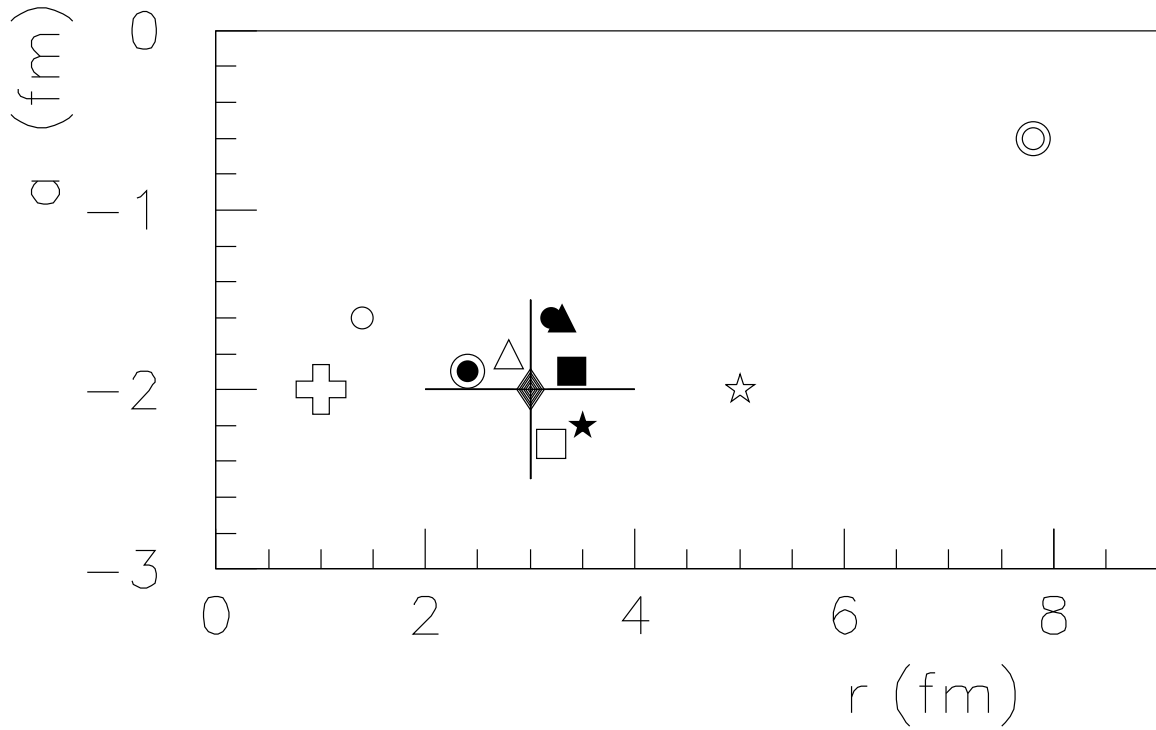


Figure 1:  $\Lambda$ - $p$  scattering parameters for the singlet and triplet states marked with open and closed symbols, respectively. Values obtained from experimental  $\Lambda$ - $p$  elastic scattering data of Refs. [1] (stars) and [2] (triangles) are shown as well as the triplet values obtained from a  $K^-$  capture experiment [4] (diamond). It is only in this latter case that an attempt was made to quote errors which are, however, strongly correlated. Points deduced from the phenomenological potential models of Refs. [5] with solution A (circles) and solution B (circles with additional outer circle) and [6] (squares) are also shown.

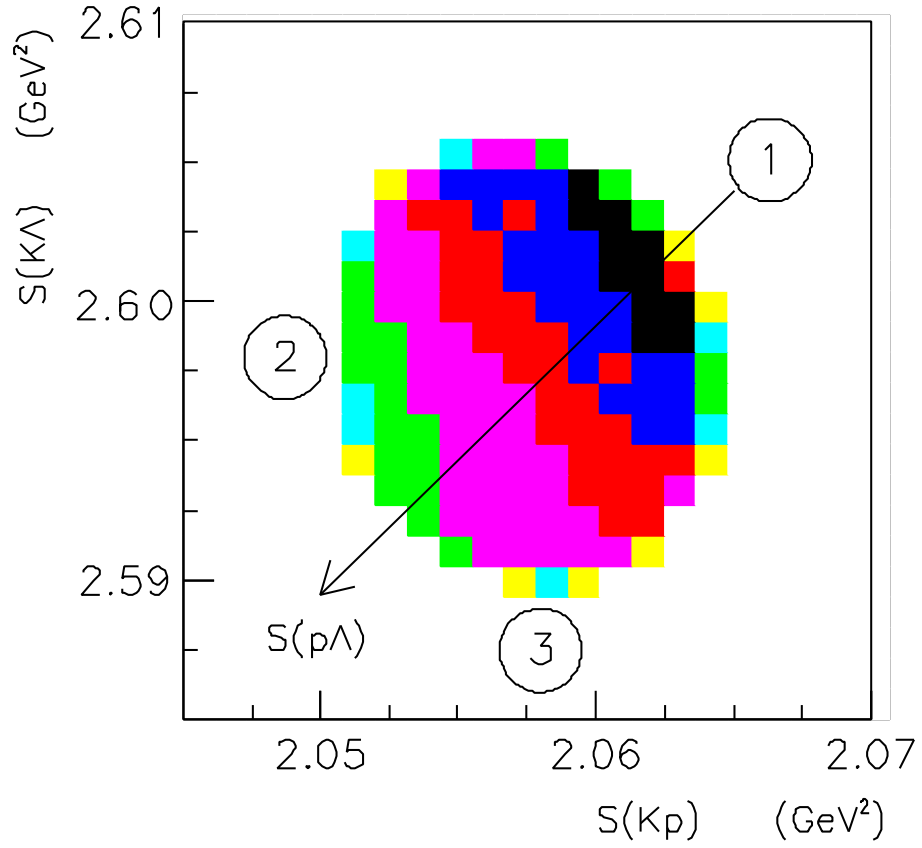


Figure 2: Monte-Carlo Dalitz plot for the  $pp \rightarrow pK^+\Lambda$  reaction at an excess energy  $\varepsilon = 4.7 \text{ MeV}$ . The numbers 1, 2, and 3 mark regions of diminishing relative energy in the  $\Lambda p$ ,  $K^+p$ , and  $K^+\Lambda$  two-body systems, respectively.

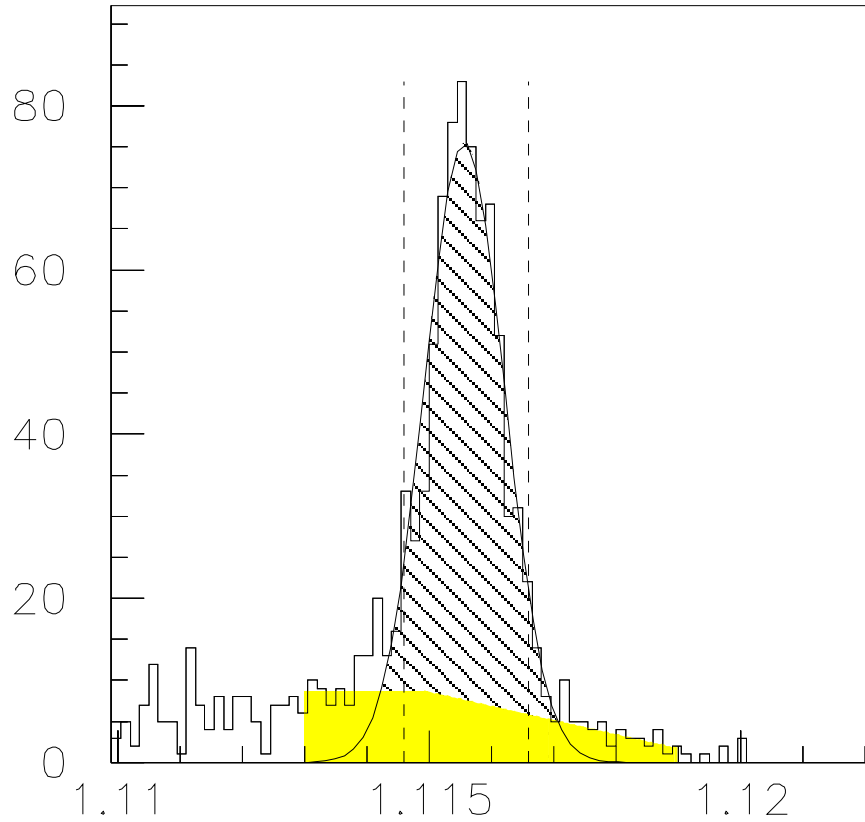


Figure 3: Experimental missing mass distribution for the  $pK^+$  subsystem from the  $pp \rightarrow pK^+X$  reaction. The fitted peak corresponds to the  $\Lambda$ -particle from the  $pp \rightarrow pK^+\Lambda$  reaction at an excess energy of  $\varepsilon = 4.7$  MeV. The grey area is an estimate of the background. Only events within the  $\pm 2\sigma$  band (dashed lines) were accepted in the final analysis.

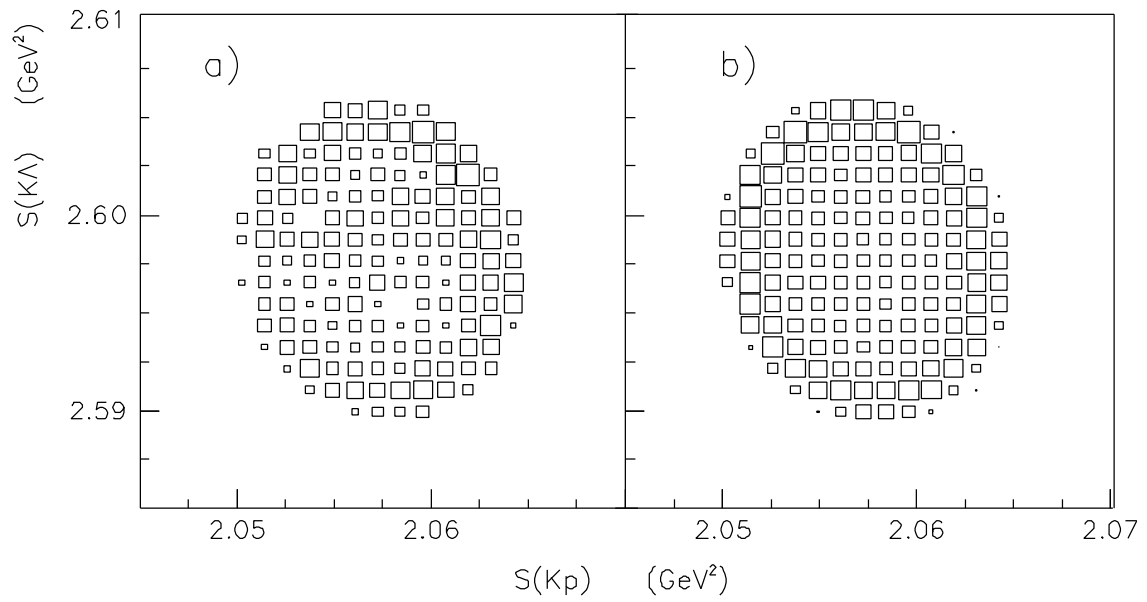


Figure 4: a) Experimental Dalitz plot at  $\varepsilon = 4.7$  MeV containing 776 events; b) The acceptance of the COSY-11 apparatus shows a typical *Colosseum*-like structure.

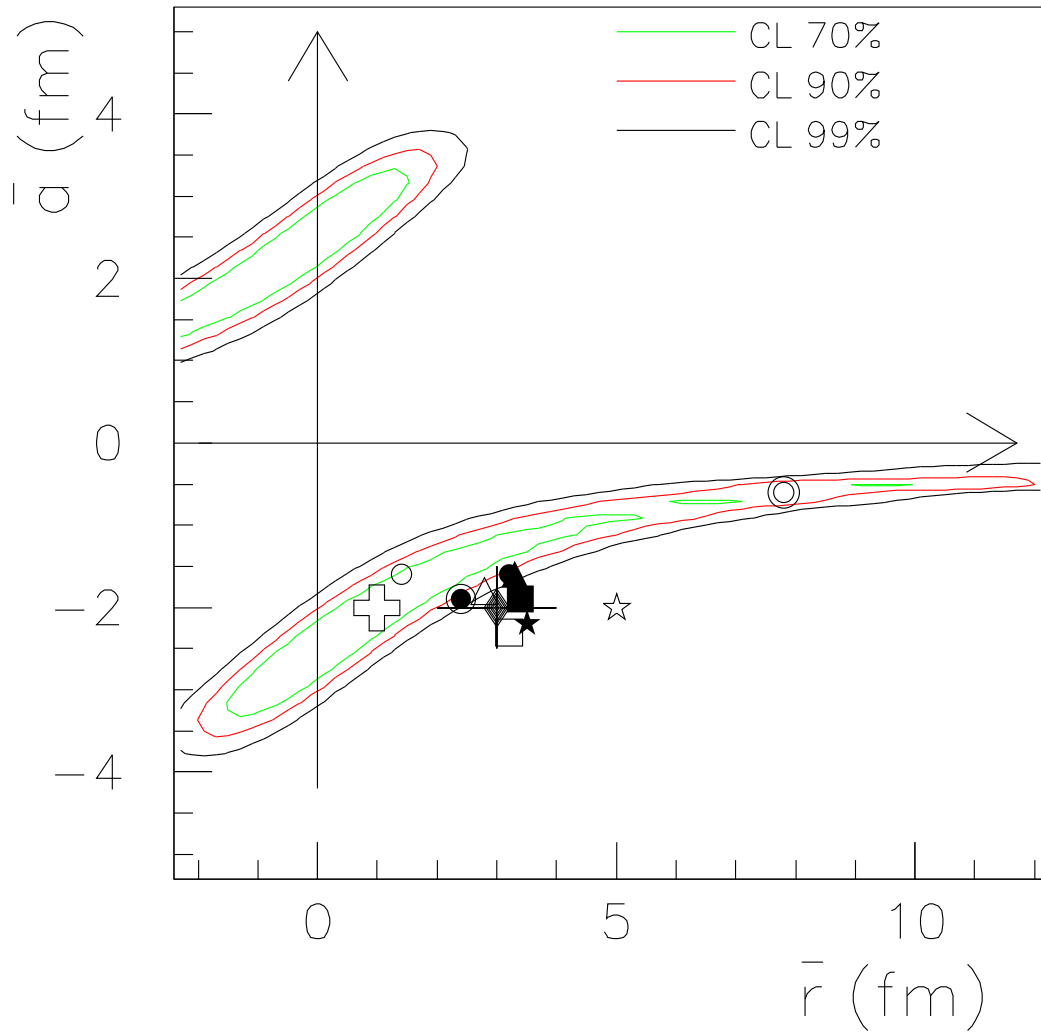


Figure 5: The logarithm of the global likelihood function  $\mathcal{L}(\bar{a}, \bar{r})$  in the  $(\bar{a}, \bar{r})$  plane obtained using all COSY-11 data measured at  $\varepsilon$  between 2.7 and 6.7 MeV. Experimental and theoretical values of these parameters are displayed using the same symbols as in Fig. 1. Combining our data with the elastic scattering data of Ref. [1,2] leads to the open cross at  $\bar{a} = -2.0$  fm and  $\bar{r} = 1.0$  fm.



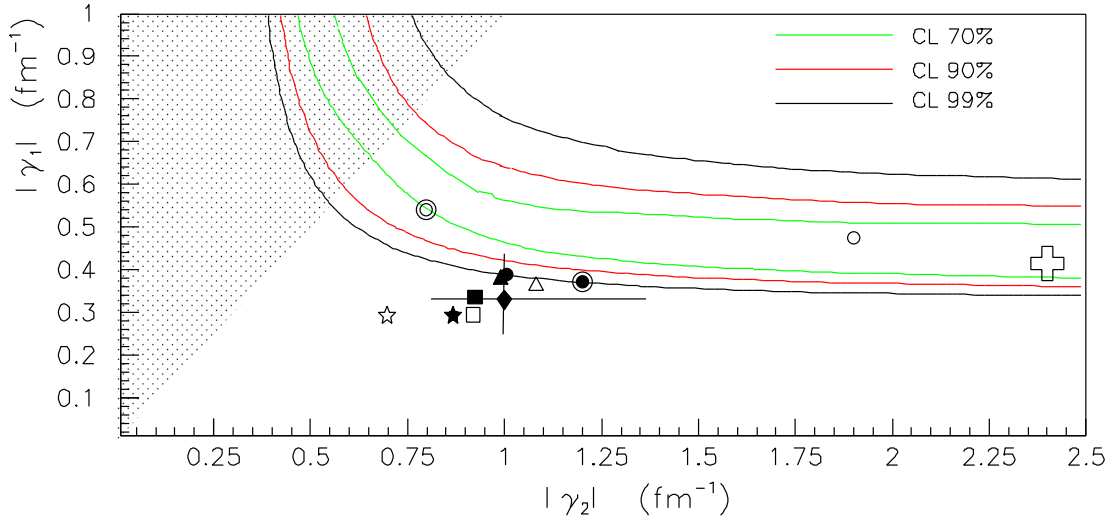


Figure 6: The global likelihood function  $\mathcal{L}(\gamma_1, \gamma_2)$  transformed into the new variables  $(\gamma_1, \gamma_2)$ . The literature values [1-6] are shown using the same conventions as in Fig. 1. Since the fit function is symmetric in  $(\gamma_1, \gamma_2)$  values, only the curves with  $\gamma_2 > \gamma_1$  are significant, and the data are insensitive to the sign of the  $\gamma_n$ . The cross at  $(0.41, 2.4)$  results from combining our data with that of low energy elastic  $\Lambda p$  scattering [1,2].

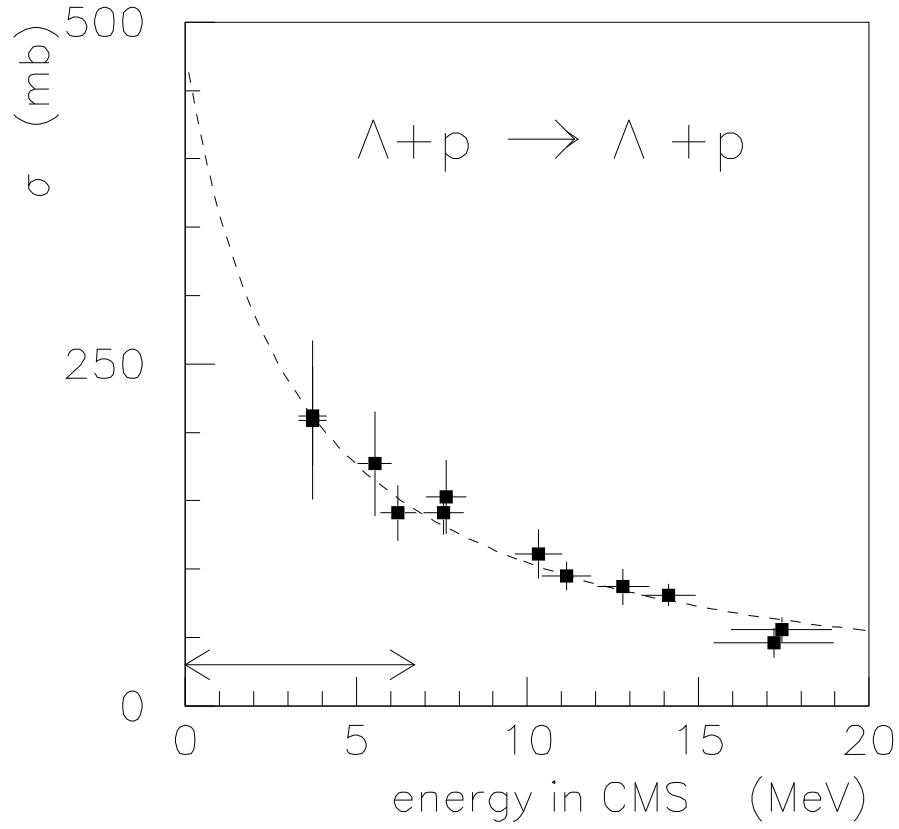


Figure 7: Low energy  $\Lambda p$  elastic scattering cross section as measured in bubble chambers [1,2] as a function of the c.m. energy  $\varepsilon$ . The arrow shows the range of energies covered by the present COSY-11 measurement. The combined fit of our data with the scattering results lead to  $\gamma_1 = -0.41 \text{ fm}^{-1}$  and  $\gamma_2 = 2.4 \text{ fm}^{-1}$  and this is shown here as the dashed line.